




The transition from used fuel container corrosion under oxidic conditions to corrosion in an anoxic environment

Elham Salehi Alaei¹  | Mengnan Guo¹ | Jian Chen¹  | Mehran Behazin² | Erik Bergendal³ | Christina Lilja³  | David W. Shoesmith^{1,4} | James J. Noël^{1,4}

¹Department of Chemistry, University of Western Ontario, London, Ontario, Canada

²Nuclear Waste Management Organization, Toronto, Ontario, Canada

³Swedish Nuclear Fuel and Waste Management Company, Solna, Sweden

⁴Surface Science Western, University of Western Ontario, London, Ontario, Canada

Correspondence

Elham Salehi Alaei and James J. Noël, Department of Chemistry, University of Western Ontario, London, ON N6A 3K7, Canada.

Email: esalehia@uwo.ca and jjnoel@uwo.ca

Funding information

Natural Sciences and Engineering Research Council of Canada; Nuclear Waste Management Organization; Swedish Nuclear Fuel and Waste Management Company, Grant/Award Number: ALLRP561193-20

Abstract

The conversion of copper oxide films on copper to copper sulfide has been investigated in sulfide-containing chloride solutions. Single-phase Cu₂O films and duplex films consisting of Cu₂O and CuO, and possibly Cu(OH)₂, were prepared electrochemically on copper specimens at various applied potentials and characterized using Raman spectroscopy, scanning electron microscopy, and energy dispersive X-ray analyses. The surface condition of the specimens subsequently exposed to a solution containing sulfide was monitored by measuring the corrosion potential (E_{corr}) for various exposure periods, then cathodic stripping voltammetry was performed. Cuprite (Cu₂O) was observed to be converted to Cu₂S by chemical reaction with sulfide, while the conversion mechanism for the mixed deposit could comprise a galvanic process involving Cu^{II} reduction coupled to the formation of Cu₂S by the reaction of sulfide with copper within pores in the Cu₂O/CuO surface film and a chemical conversion of Cu₂O to Cu₂S. Cupric hydroxide was not converted to Cu₂S on the time scale (24 h) of these experiments.

KEYWORDS

cathodic stripping, conversion, copper, corrosion, nuclear fuel waste management, oxide, sulfide

1 | INTRODUCTION

Globally, nuclear is considered the second largest source of low-carbon power.^[1] The used nuclear fuel, however, constitutes a chemical and radiological hazard to human health and the environment.^[2,3] Hence, to continue the use and development of nuclear power for electricity generation, it is imperative that the used nuclear fuel should be safely managed. The internationally accepted approach for the safe and long-term management of used nuclear fuel is to dispose of it in sealed metallic containers in a deep

geological repository (DGR) at a depth of approximately 500–800 m in a stable geological formation.^[4,5] The long-term safety of a DGR strongly depends on the survival of its natural and engineered barriers over a million of years. The key engineered barrier is the used fuel container (UFC), which is typically surrounded by swelling bentonite clay that serves to seal up the DGR. In Canada, the UFC consists of a strong carbon steel vessel coated with a 3-mm-thick layer of copper (Cu). Cu has been chosen as the main corrosion barrier for the container in Finland, Sweden, Canada, and some other countries (e.g., Switzerland, South

This is an open access article under the terms of the Creative Commons Attribution-NonCommercial-NoDerivs License, which permits use and distribution in any medium, provided the original work is properly cited, the use is non-commercial and no modifications or adaptations are made.

© 2023 The Authors. *Materials and Corrosion* published by Wiley-VCH GmbH.

Korea, and Japan) are considering Cu coating due to its known corrosion resistance under anoxic conditions.^[2,6–11]

Cu containers emplaced in a DGR will experience an evolution of exposure conditions. Initially, the environment in the vicinity of the container will be oxidizing and warm due to limited amounts of trapped O₂ during the construction phase and heat from radioactive decay within the fuel matrix. Under these conditions, corrosion will lead to the formation of oxide layers on the Cu surface.^[12,13] Presently available information indicates that the maximum depth of container corrosion due to O₂ consumption will be limited to 298 μm, as calculated using mass balance, conservatively assuming the corrosion product to be Cu₂O only. Additionally, oxidants produced by H₂O radiolysis could result in a further 10–30 μm penetration of the Cu coating.^[14,15] Once anoxic conditions are established, SH[−] produced by the action of sulfate-reducing bacteria could diffuse through the sealing system and cause Cu corrosion.^[16–18] In Swedish/Finnish and Canadian DGRs, the groundwater SH[−] concentrations are expected to be up to 10^{−4} and <10^{−6} M, respectively.^[8,19]

Considerable efforts have been dedicated to investigating Cu corrosion in SH[−] environments under anoxic conditions; however, this has concentrated on determining the kinetics and mechanism of copper sulfide film growth (as chalcocite (Cu₂S)) and quantifying the key parameters that influence film formation.^[20,21] In addition to [SH[−]], the transport of SH[−] to the Cu surface also plays a role in determining the morphological and protective properties of the sulfide film formed on the Cu surface.^[21] Martino et al.^[22] categorized the properties of Cu₂S films formed at different [SH[−]] and [Cl[−]], the latter anion being expected to be particularly important in Canadian groundwater composition. The same author showed that as the [SH[−]] increased, the sulfide film evolved from a single-layer porous film to a partially passivating film. In addition, Cl[−] ions were found to influence the Cu corrosion in different ways: (a) Cl[−] displaced adsorbed SH[−] from the Cu surface, which inhibits the initial step in the sulfide film formation process; (b) Cl[−] induced and maintained porosity in the sulfide film; and (c) at very high concentration (i.e., 5.0 M), Cl[−] could facilitate Cu transport as CuCl₂[−] and other such complexes.^[22–24]

To date, the influence of the initial oxidic phase anticipated in a DGR on the subsequent Cu corrosion by SH[−] has not been studied in detail. Kristiansen et al.^[25] investigated the sulfidization of copper oxide, both in the form of a layer grown on metallic Cu and as a powder, using soft X-ray spectroscopy. The results demonstrated that the tenorite (CuO) layer on the oxidized Cu surface reacted with the SH[−] solution, with the top 100 nm layer of oxide being converted to Cu₂S in a transformation involving the reduction of Cu^{II} to Cu^I-containing species.

By contrast, the transformation of CuO powder to Cu^I species was much less pronounced. Although the mechanism for the reduction of Cu^{II} to Cu^I was not clearly understood, it was proposed that the main mechanism was likely the comproportionation reaction between Cu atoms in the underlying metallic Cu and Cu^{II} ions from the corrosion products. If this mechanism prevailed, the absence of Cu metal in the experiments with powdered oxide would prevent the transformation of Cu^{II} to Cu^I, consistent with observations.

King et al.^[26] conducted a simulation of evolving repository redox conditions with a focus on the impact of microbiological processes on Cu corrosion. As conditions evolved from oxidic to anoxic, a shift in E_{corr} to less noble (less positive) values was observed. As the [SH[−]] was increased, E_{corr} approached a value in the range of −0.8 to −1.0 V/saturated calomel electrode (SCE). Experiments conducted on a stationary electrode covered by a clay layer yielded similar results but with a delayed response of the E_{corr} to the presence of SH[−] due to the slow mass transport of SH[−] through the clay.

Smith et al.^[27] showed that the composition of the electrochemically formed oxide film on Cu varied from a compact Cu₂O film, after short periods of oxidation, to a porous trilayer film composed of a Cu₂O base layer, a thin intermediate layer of CuO, and an outer scattered deposit of Cu(OH)₂ after longer oxidation periods. Scanning electron micrographs of specimens indicated that the coherent oxide layer formed after 0.5 h was converted to a porous layer covered by scattered surface deposits after an additional 2 h. On the basis of the evolution of the E_{corr} with time, Smith et al. showed that upon exposure of preoxidized Cu samples to SH[−], conversion of the oxide to sulfide was observed. This was confirmed by in situ Raman spectroscopy and cathodic stripping voltammetry. It was claimed that this conversion occurred by chemical conversion of oxide to sulfide at the oxide/electrolyte interface. The sulfide films on the preoxidized Cu surface continued to grow, yielding dendritic sulfide crystals on top of the oxide layer until, at longer times, the surface became covered by a porous sulfide layer.

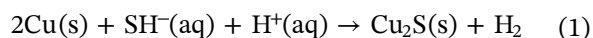
Abd El Haleem and Abd El Aal^[28] investigated the electrochemical behavior of Cu in SH[−]-containing 0.1 M NaOH solutions. Galvanostatic polarization of Cu specimens was performed in solutions containing SH[−] in the range of 10^{−6}–5 × 10^{−3} M. For [SH[−]] ≤ 5 × 10^{−5} M, potential–time profiles were similar to those measured in the absence of SH[−] and, based on reduction potentials, Cu₂O, CuO, and/or Cu(OH)₂ were thought to have been formed. It was proposed that there may be an [SH[−]] threshold below which Cu^I sulfide formation would be kinetically hindered.

Hollmark et al.^[29] grew either Cu^I or Cu^{II} films, exposed them to solutions containing either 10⁻³ or 0.1 M sodium sulfide (Na₂S) for 8 h, and then analyzed the surfaces using X-ray absorption spectroscopy (XAS). They observed sulfide diffusion into the bulk oxide films but suggested that this process proceeded inhomogeneously since a small amount of oxide film remained unconverted. The findings demonstrated that the sulfide films formed were not coherent layers. In agreement with Smith et al.,^[27] it was concluded that oxide-to-sulfide conversion could occur by different conversion mechanisms.

While these studies show that Cu oxides will eventually be converted to sulfides, the mechanisms of conversion and the involvement of the metallic Cu substrate remain unresolved. A number of possible corrosion scenarios can be envisaged to occur when SH⁻ contacts a preoxidized waste container surface:

1. No conversion of copper oxide to sulfide

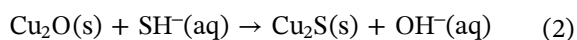
The SH⁻ could cause Cu corrosion, reaction (1), by transport through the porous oxide without reacting with it:



This would yield the maximum amount of container corrosion since only the metallic Cu would consume the SH⁻.

2. Chemical conversion of oxide to sulfide

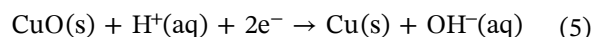
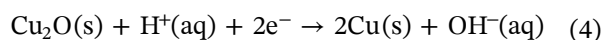
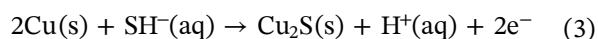
The conversion of Cu₂O to Cu₂S could occur via a chemical substitution reaction, reaction (2), between SH⁻ and the oxide, with no redox reaction involved.



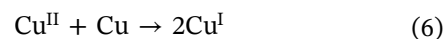
Reaction with the oxide would initially consume SH⁻ transported to the container surface, thereby delaying further Cu corrosion. This would decrease the extent of corrosion to the container since sulfide-driven Cu corrosion would only initiate either after the oxide layer was totally consumed by reaction with SH⁻ or when it became sufficiently porous to allow SH⁻ transport to the underlying metal.

3. Electrochemical conversion of oxide to sulfide

The transport of SH⁻ to the container surface through a porous oxide could result in oxidation of Cu by SH⁻, reaction (3), galvanically coupled to the simultaneous reduction of the oxide, reactions (4) and (5):



In this scenario, the amount of Cu consumed in forming Cu₂S would be the same as that produced by the reduction of the copper oxide. However, Cu produced by oxide reduction would be expected to be finely particulate and unprotective and eventually converted to Cu₂S via reaction (3). Additionally, in the presence of Cu^{II} species, Cu produced could participate in the comproportionation reaction to reduce Cu^{II} to Cu^I via reaction (6):



with Cu^I leading to Cu₂S formation via reaction (3) or Cu₂O by reaction with H₂O.

4. A combination of all possible interactions

A possibility is that some of the SH⁻ may be consumed in converting oxide (either chemically or galvanically) to sulfide while the remainder penetrated the porous oxide to directly corrode the underlying Cu substrate. The subsequent amount of Cu corrosion would be decreased by the amount of SH⁻ consumed in the conversion process, which would depend on the degree of conversion of oxide to sulfide, a reaction that may or may not go to completion.

This range of mechanistic possibilities makes it necessary to evaluate the mechanism and extent of oxide conversion to sulfide and how it influences the maximum depth of corrosion damage to the container. In this study, the mechanism and extent of conversion of different types of copper (hydr)oxides with known compositions and thicknesses were investigated. This was achieved by preoxidizing Cu to form oxide layers with known compositions representative of the oxic period, then exposing them to oxygen-free solutions containing a known concentration of SH⁻, simulating the anoxic environment. The extent of oxide-to-sulfide conversion was then analyzed using cathodic stripping voltammetry and a range of surface analytical techniques.

2 | EXPERIMENTAL

2.1 | Sample preparation

O-free, P-doped (0.003–0.01 wt%) wrought Cu provided by SKB, Swedish Nuclear Fuel and Waste Management Company, was used in all experiments. The Cu samples were machined into 1-cm-diameter disks, threaded and connected to a Ti rod. The disks were set in

polytetrafluoroethylene holders using epoxy resin (Hysol EE4190 GAL CZZ 0001 JF, Henkel) with only a single flat circular face with a total surface area of 0.785 cm² left bare to be exposed to the electrolyte. The disks were ground using a sequence of SiC papers (800, 1000, 1200, 2500, and 4000 grit), polished to a mirror finish using a 1- μ m diamond suspension, rinsed with Type-I water, ultrasonically cleaned with methanol, washed again with Type-I water, and finally dried in a stream of Ar gas.

2.2 | Electrochemical/corrosion cell design and instrumentation

In all experiments, a conventional three-electrode electrochemical cell was used. A Pt sheet connected to external circuitry with a Pt wire and an SCE (0.242 V/Standard Hydrogen Electrode) were used as the counter and reference electrodes, respectively. Periodically, the SCE was checked against a master reference SCE to ensure the electrode remained reliable. Potentials were controlled and currents were measured using a Solartron Analytical Modulab equipped with Corrware (Scribner Associates) and XM-Studio-ECS software.

2.3 | Electrolyte preparation

All solutions were prepared with Type-1 water (resistivity: 182 k Ω m) that was purified using a Barnstead Nanopure water system. Reagent-grade NaOH (assay 98.9%, Fisher Chemical) was used to make the 0.1 M solutions used in preparing oxide-coated electrodes. Reagent-grade sodium sulfide (Na₂S·9H₂O, assay \geq 98.0%, Sigma Aldrich) was used to prepare solutions with a total [SH⁻] of 5 \times 10⁻⁵ M. Since Na₂S is stored in hydrated form, it was first dried to minimize errors in calculating concentrations. All SH⁻ solutions contained 0.1 M NaCl (assay \geq 99.0%, Fisher Chemical) as a supporting electrolyte.

2.4 | Electrochemical/corrosion experiments

All experiments were conducted inside a Faraday cage to decrease electrical noise from external sources. Before experiments, solutions were sparged with a stream of ultrahigh purity Ar gas for 20 min with sparging continued throughout the experiment. The Cu electrodes were cathodically cleaned at -850 mV/SCE for 3 min before each experiment.

2.4.1 | Cyclic voltammetry

The voltammetric experiment was performed to investigate the mechanism of copper (hydr)oxide formation. The potential was scanned from -1.3 to 0.5 V/SCE at a scan rate of 1 mV/s under deaerated conditions to identify the appropriate potentials to be used in film growth experiments.

2.4.2 | Potentiostatic polarization

Freshly prepared Cu specimens were oxidized at -0.3 and -0.22 V/SCE in 0.1 M NaOH solution for 30 min, under deaerated conditions, to form oxides with different compositions. When used in subsequent experiments involving exposure to SH⁻-containing solutions, these specimens are described as preoxidized.

2.4.3 | Corrosion potential measurements

Corrosion potentials (E_{corr}) were monitored on preoxidized samples after transfer to a second electrochemical cell containing SH⁻ solutions to investigate the effect of SH⁻ on the preformed oxide films.

2.4.4 | Cathodic stripping voltammetry

After E_{corr} measurement of various durations in SH⁻ solutions, the potential was scanned from the final value of E_{corr} to -1.4 V/SCE at a scan rate of 1 mV/s to cathodically strip oxide and sulfide films present on the electrode surface. The negative potential limit was chosen to minimize the onset of H₂ evolution due to H₂O reduction. From the potentials at which cathodic peaks appeared and the measured charges associated with them, the nature and amount of the oxide and sulfide phases present were determined.

2.5 | Surface analyses

2.5.1 | Laser Raman spectroscopy

The phases present on the preoxidized Cu samples before and after exposure to SH⁻ solutions were analyzed using laser Raman spectroscopy. Raman spectra were collected using a Renishaw InVia Reflex Raman spectrometer equipped with a He-Ne laser with a wavelength of 632.8 nm to excite Raman active vibrations. Spectra were recorded over the wavelength shift range of 150–900 cm⁻¹,

with the laser used at 5% power to minimize any surface heating effects. All Raman spectra reported in this manuscript include the raw data only.

2.5.2 | Scanning electron microscopy (SEM)

Surface imaging was performed using either a Hitachi SU8230 Regulus Ultra High-Resolution Field Emission SEM (FE-SEM) equipped with energy dispersive X-ray spectroscopy (EDX) or a Hitachi SU3500 Variable Pressure SEM combined with an Oxford Aztec X-Max50 SDD X-ray analyzer. EDX was carried out to elucidate the elemental composition of the surface. All SEM/EDX analyses were performed using an accelerating voltage of 5–10 keV with a spot intensity of 50%–70%.

An LEO (Zeiss) 1540XB focused ion beam (FIB) coupled with SEM was used to section samples using a Ga ion beam and to obtain cross-sectional images of surface films.

3 | RESULTS AND DISCUSSION

3.1 | Voltammetric behavior of Cu in deaerated 0.1 M NaOH solution

A cyclic voltammogram was recorded on Cu in an Ar-sparged solution (pH 12.9), Figure 1, to determine the conditions required to grow different types of copper oxides. During the positive-going scan, the first small anodic peak (blue region A in Figure 1) is attributed to

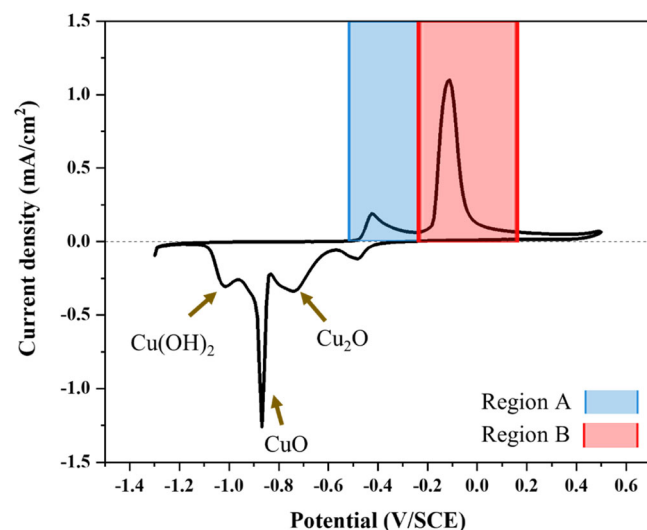
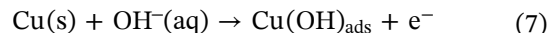


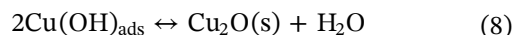
FIGURE 1 Cyclic voltammogram recorded at a scan rate of 1 mV/s on a Cu electrode in 0.1 M NaOH solution under deaerated conditions. Regions A and B represent different oxidation processes.

the formation of a thin film of Cu_2O on the Cu surface. Strehblow et al.^[30] showed that, before film formation, for $E > \sim -0.8$ V/SCE, OH^- adsorption on the surface occurs, reaction (7):

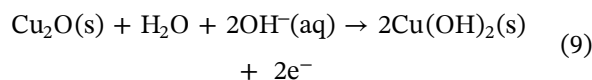


which leads to an irreversible surface reconstruction as OH^- is adsorbed–desorbed.^[30,31]

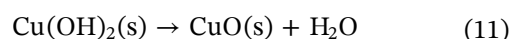
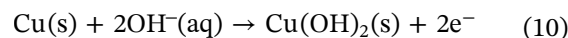
The formation of the Cu_2O layer, reaction (8), starts with the growth of small disk-like features, preferentially located at the terrace step edges, which eventually cover the whole surface.^[31,32]



At more oxidizing potentials, a second peak is observed (red region B in Figure 1). This peak has been attributed to the further oxidation of Cu^0 and Cu_2O to yield a $\text{Cu}_2\text{O/CuO/Cu(OH)}_2$ layer, reactions (9)–(11).^[27,30] At sufficiently high potentials ($> \sim 0.2$ V/SCE), partial passivation of the electrode surface occurs and hinders further oxidation^[27]:



and



On the basis of this voltammetric evidence, one would expect that applying a film growth potential in region A would result in the formation of a thin single-phase Cu^{I} oxide layer, while applying a potential in region B would lead to the formation of a much thicker duplex layer of Cu^{I} and Cu^{II} oxide or Cu^{II} hydroxide on the Cu surface.

As shown in Figure 1, on the negative-going scan, the cathodic peaks can be attributed to the reduction of Cu_2O , CuO , and Cu(OH)_2 films, respectively, as described previously by Smith et al.^[27] It appears that the cathodic peak for Cu_2O was preceded by a small peak which can be related to either an adsorbed layer or a defective form of Cu_2O layer on the Cu surface.

3.2 | Formation of a single-layer Cu_2O film

To find the most appropriate potential to form a layer of single-phase Cu_2O on the Cu surface, oxide growth at

three different potentials in region A (-0.43 , -0.40 , and -0.3 V/SCE in Figure 1) was evaluated. Figure 2 shows the current–time relationships recorded. At -0.43 V/SCE, the current density appeared to be about to switch to a negative value at longer times. For the two more positive applied potentials, the current density approached a low,

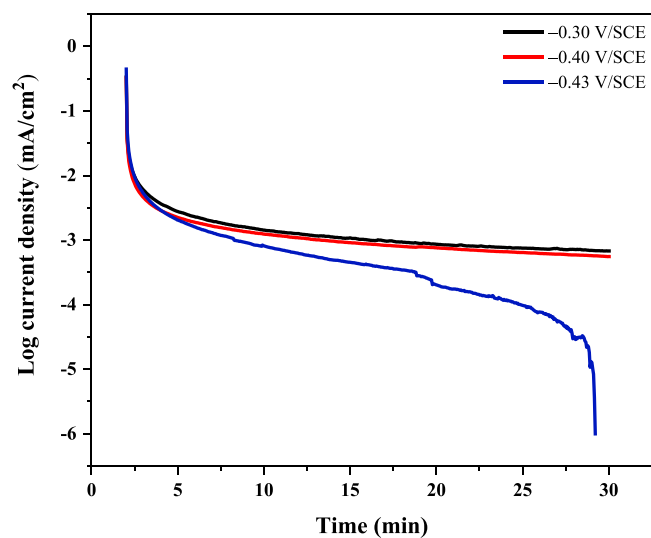


FIGURE 2 Log current density as a function of time for anodic polarization of Cu samples at different potentials in 0.1 M NaOH solution in region A in Figure 1.

TABLE 1 Absolute charge densities calculated by integration of the current density–time curves in Figure 2.

Applied potential (V/SCE)	Charge density ($\mu\text{C}/\text{cm}^2$)
-0.30	4423
-0.40	3880
-0.43	3830

constant, potential-independent value at longer times. Integrating the current density–time transients yields a measure of the extent of film formation, assuming no dissolution as soluble Cu^{I} has occurred.^[33] On the basis of these results, -0.3 V/SCE was chosen as a suitable potential for the growth of the thickest single-phase Cu_2O layer. This choice is based on the higher charge density for film formation observed, Table 1.

Figure 3 shows SEM micrographs of the surface morphology of a film grown at -0.3 V/SCE. A thin uniform and featureless film is observed (Figure 3a), with the ridges from the surface preparation still observable (Figure 3b) confirming that the film is thin. The Raman spectrum in Figure 4 shows two broad peaks at 523 and 623 cm^{-1} and one small peak at 218 cm^{-1} , confirming the presence of Cu_2O ,^[33,34] with no indication of the presence of any other oxide/hydroxide.

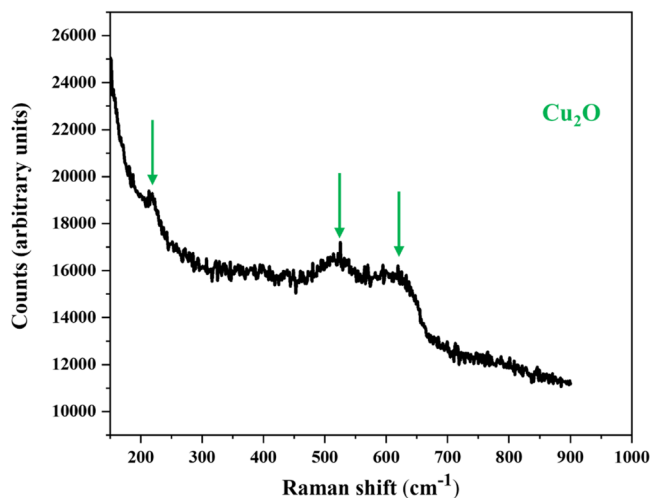


FIGURE 4 Raman spectrum recorded on a Cu sample preoxidized at -0.3 V/SCE in deaerated 0.1 M NaOH solution.

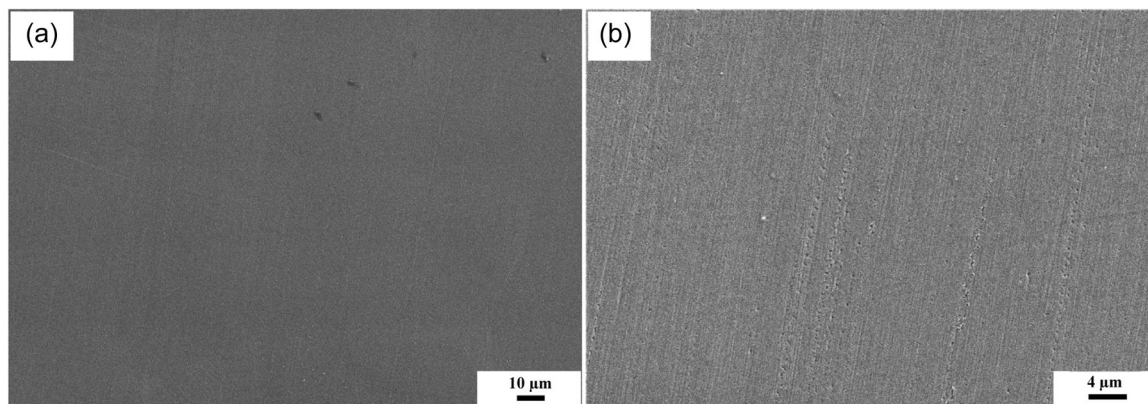


FIGURE 3 Morphology of an oxide film anodically grown at -0.3 V/SCE on the Cu surface in 0.1 M NaOH solution at different magnifications (a) $\times 600$, (b) $\times 2.00\text{k}$.

The thickness of the oxide layer formed (δ) can be calculated using the charge densities in Table 1 and Faraday's law, Equation (12),

$$\delta = \frac{q}{nF} \times V_m \quad (12)$$

where q is the charge density (C/m^3), V_m the molar volume of the oxide ($2.39 \times 10^{-5} m^3/mol$ for Cu_2O), n the number of exchanged electrons, and F the Faraday constant ($96,485 C/mol$).^[32] On the basis of Equation (12), the average thickness of the Cu_2O layer formed on Cu after anodic polarization at $-0.3 V/SCE$ for 30 min was around 10 nm.

3.3 | Formation of a duplex Cu_2O - CuO ($Cu(OH)_2$) film

The oxide film formed on a UFC emplaced in a DGR is expected to be a combination of Cu^I and Cu^{II} products. Thus, to study an oxide film more closely, simulating those that will grow under the expected DGR conditions, Cu specimens were anodically polarized for 30 min at a number of more oxidizing potentials than that used to grow a Cu_2O film and then cathodically stripped to determine the phases formed. Figure 5 shows cathodic stripping voltammograms (CSVs) recorded after oxidation at different potentials. If the potential was set at either -0.3 , -0.27 , or $-0.24 V/SCE$, only a single small reduction peak was observed, at $\sim -0.67 V/SCE$, Figure 5b, consistent with the formation of a very thin

layer of Cu_2O as observed in Figure 3 and demonstrated in the Raman spectrum in Figure 4. Oxidation at $-0.22 V/SCE$ led to an additional much larger reduction peak at $\sim -0.9 V/SCE$, which suggests the presence of CuO as indicated in the CV in Figure 1 and proposed by Smith et al.^[27] After oxidation at $-0.20 V/SCE$, the observation of a third reduction peak at $\sim -1.2 V/SCE$ indicates the formation of $Cu(OH)_2$, based on Figure 1 and the analysis of Smith et al.^[27] Figure 5b shows a very small shoulder in the reduction current density in the potential region more negative than $\sim -0.85 V/SCE$, suggesting the onset of the formation of Cu^{II} phases. This confirms the choice of $-0.3 V/SCE$ as the most appropriate potential to form a single layer of Cu_2O in experiments in which SH^- was subsequently added (below).

The morphological properties of the multiphase film formed at $-0.22 V/SCE$ are shown in the SEM images of the surface and the cross section in Figure 6. The surface images show a uniform coverage of two-dimensional crystals with a sparse outer distribution of rod-like features. The cross section shows a film thickness of ~ 208 nm, compared with the ~ 10 -nm-thick layer of Cu_2O formed at $-0.3 V/SCE$. The Raman spectrum in Figure 7 shows a series of peaks and shoulders, indicating that the film was composed of a mixture of phases. As shown in Figure 4 and discussed in reference,^[35] Cu_2O yields peaks at 530 and $623 cm^{-1}$, as well as a minor peak at $220 cm^{-1}$. The dominance of the broad peak at $\sim 620 cm^{-1}$, compared with the shallow shoulder at $\sim 530 cm^{-1}$ and the sharp peak at $300 cm^{-1}$ followed by a small peak at $350 cm^{-1}$,

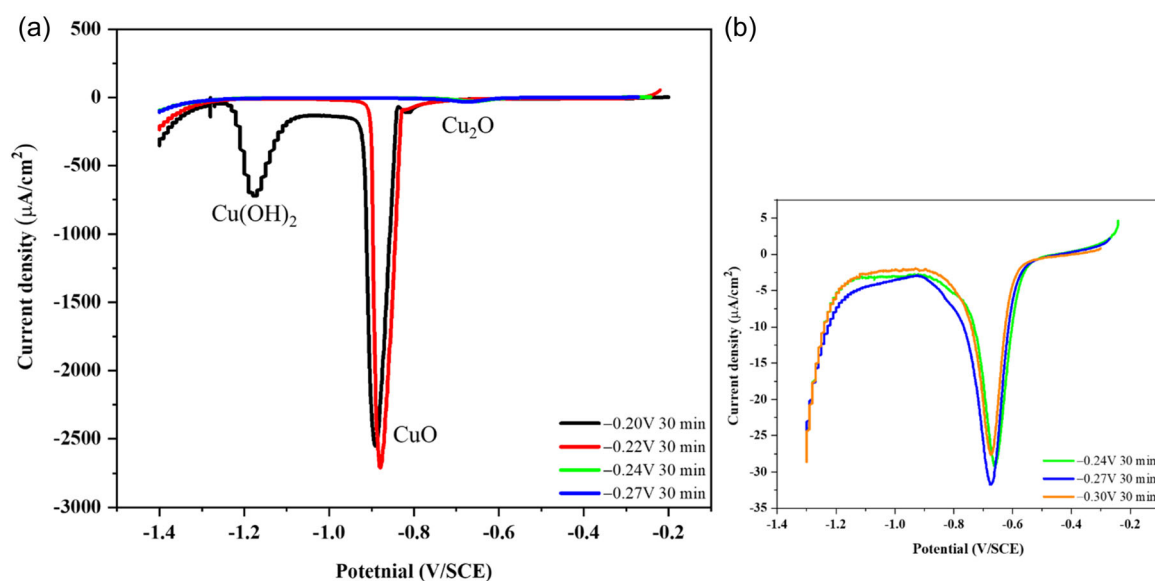


FIGURE 5 (a) Cathodic stripping voltammograms (CSVs) on Cu samples after anodic polarization at different potentials in 0.1 M NaOH solution, (b) CSVs recorded after oxide growth at -0.24 , -0.27 , and $-0.3 V/SCE$ on an enhanced current density scale.

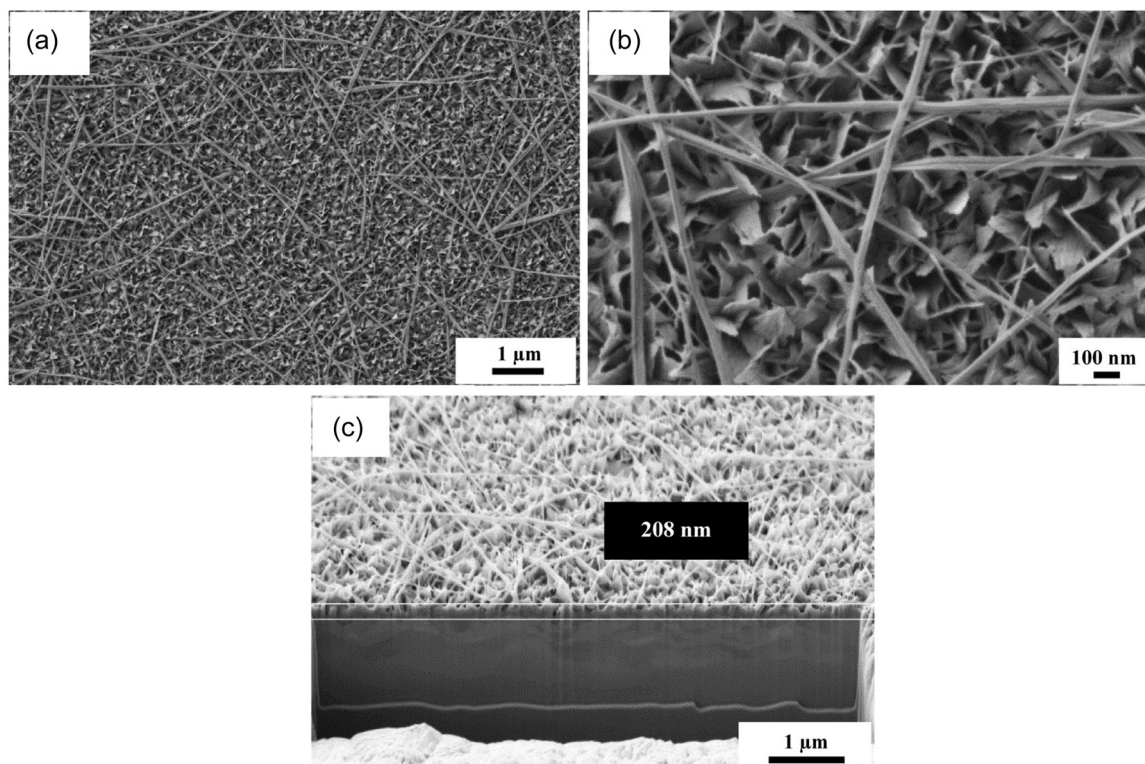


FIGURE 6 FE-SEM micrographs (a, b) showing the surface morphology of an oxide film anodically grown at -0.22 V/SCE in 0.1 M NaOH solution and (c) an FIB-cut cross section of the film.

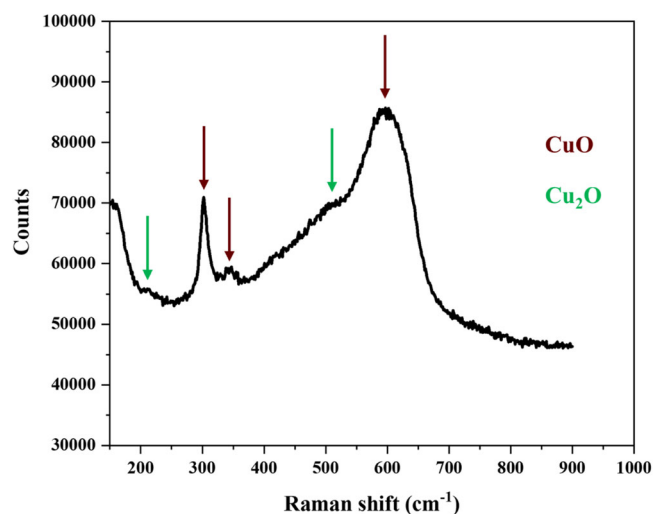


FIGURE 7 Raman spectrum recorded on a Cu sample preoxidized at -0.22 V/SCE in deaerated 0.1 M NaOH solution.

indicates the presence of CuO , which also exhibits a peak at ~ 635 cm^{-1} .^[35,36] Although not well defined, the shoulder in the region of 400 – 550 cm^{-1} could contain a contribution from $\text{Cu}(\text{OH})_2$, which would yield a peak in the region of 460 – 490 cm^{-1} .^[36] It is feasible that such a

weak signal could indicate that the dispersed layer of rod-like crystals is $\text{Cu}(\text{OH})_2$ while the main body of the film is a mixture of Cu_2O and CuO . The size of the reduction peak at ~ -0.9 V/SCE in the CSV (Figure 5a) suggests that CuO may be the dominant phase present, although it is also feasible that further formation of Cu_2O is promoted by reaction (6).

3.4 | Conversion of Cu_2O to Cu_2S

Cu samples preoxidized at -0.3 V/SCE for 30 min were immediately transferred to another electrochemical cell and E_{corr} monitored for various durations in deaerated 0.1 M $\text{Cl}^- + 5 \times 10^{-5}$ M SH^- solution, Figure 8a. The initial E_{corr} values for the individual experiments were in the range of -0.36 to -0.4 V/SCE, which is more negative than the potential for the $\text{Cu}/\text{Cu}_2\text{O}$ equilibrium, suggesting some porosity in the Cu_2O layer. E_{corr} decreased slowly for a period that varied in duration for the three samples before E_{corr} underwent a transition to -0.85 V/SCE, a value close to the potential for the $\text{Cu}/\text{Cu}_2\text{S}$ equilibrium at the specific concentration used in this experiment, demonstrating that the Cu surface was exposed to SH^- and E_{corr} controlled by the $\text{Cu}/\text{Cu}_2\text{S}$ reaction.

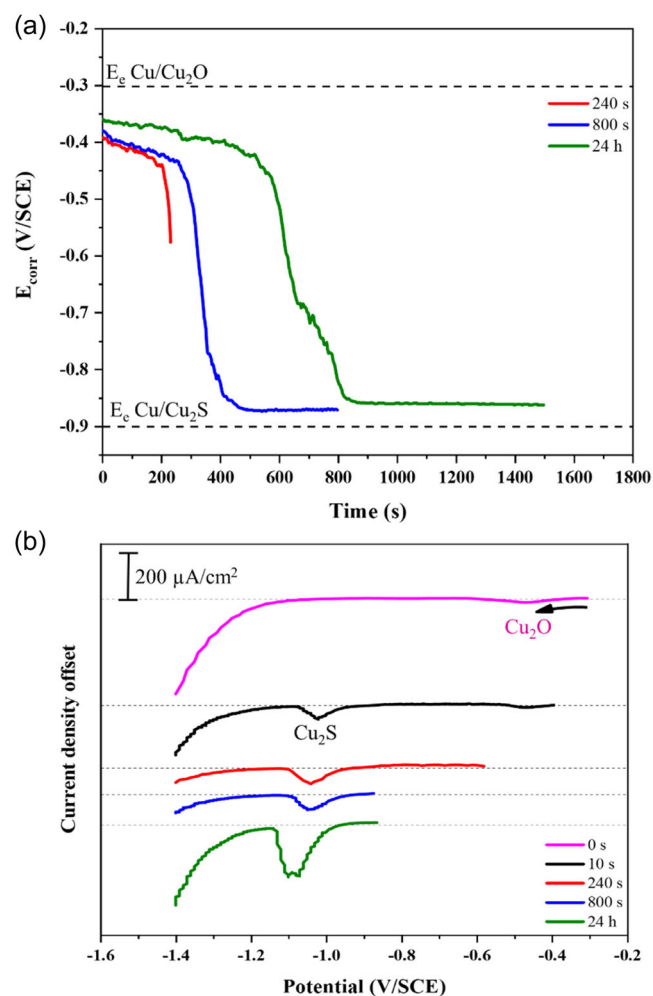


FIGURE 8 (a) E_{corr} recorded on Cu samples preoxidized at -0.3 V/SCE in 0.1 M NaOH solution after immersion in anaerobic solutions containing 0.1 M $\text{Cl}^- + 5 \times 10^{-5}$ M SH^- (variations show the inherent irreproducibility of transition times and reproducibility of potentials) and (b) the respective CSVs performed at a scan rate of 1 mV/s after the surface was exposed to the sulfide solution for different time periods, as indicated.

After each period of immersion, a CSV was performed to determine the nature and amount of the phases present on the exposed surface, Figure 8b. Also shown are CSVs recorded on a specimen exposed for only 10 s and one preoxidized but not subsequently exposed to an SH^- -containing solution. Before exposure to the SH^- solution, only a thin Cu_2O film, cathodically reduced in the range of -0.4 to -0.5 V/SCE, was present on the Cu surface. This reduction peak disappeared after a short SH^- exposure period and was replaced by a peak at potentials < -1.0 V/SCE, indicating Cu_2S reduction.^[22,23]

The anodic charge densities accumulated during the oxidation step and the cathodic charge densities calculated by integrating the oxide and sulfide reduction peaks in the CSVs in Figure 8b are shown in Figure 9. For the blank experiment, the difference between the oxidation charge and cathodic charge (which averaged $5\% \pm 1\%$ over three repeat runs) is a result of rinsing with Type-I water before transferring to the cell containing sulfide solution. To verify this finding, a two-step blank experiment including the oxide formation and cathodic stripping of the formed film was performed in the same solution (0.1 M NaOH). The cathodic charge obtained from CSV was equal to the calculated anodic charge. Since the oxidation state of the Cu (Cu^1) is the same in both the preformed oxide (Cu_2O) and the Cu_2S conversion product, the charges obtained are directly comparable. Most of the oxide was converted to sulfide in the first 20 s, with the subsequent increase in total charge indicating that SH^- oxidation of the substrate Cu to Cu_2S begins before the conversion of Cu_2O is complete and continues after the conversion is complete. The continuous long-term growth of Cu_2S is consistent with the results of previous corrosion studies.^[37]

The SEM micrograph of the film formed after an extensive exposure of 24 h, Figure 10, shows that it was composed of a uniformly distributed granular deposit,

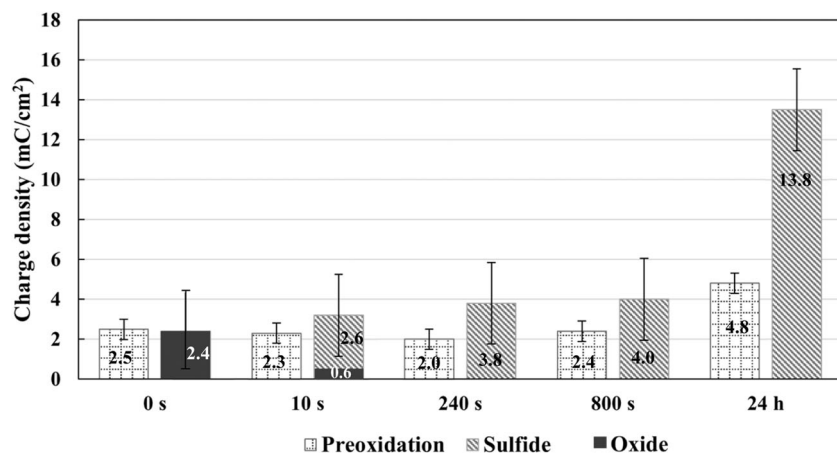


FIGURE 9 Anodic charge densities for samples preoxidized at -0.3 V/SCE in 0.1 M NaOH solution and the corresponding cathodic charges, with standard deviation, after immersion for different periods of time in a solution containing 0.1 M $\text{Cl}^- + 5 \times 10^{-5}$ M SH^- .

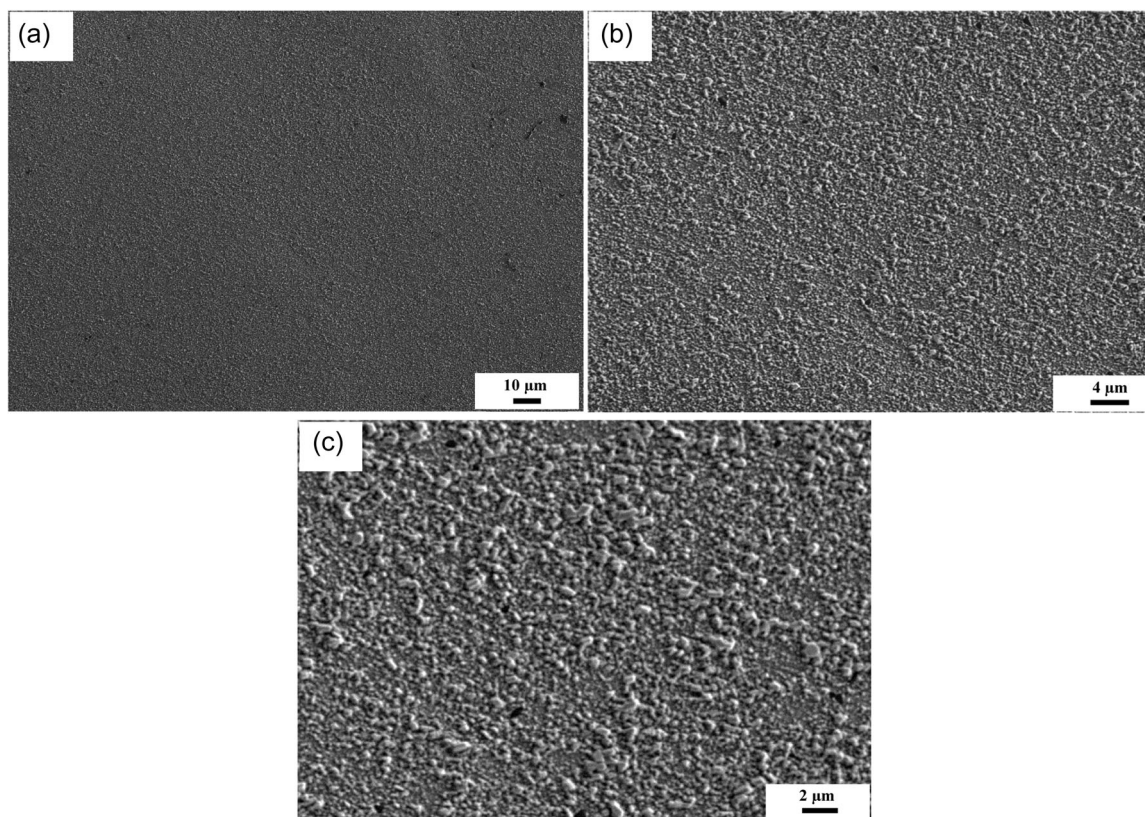


FIGURE 10 Morphology of the oxide film grown anodically at -0.3 V/SCE on the Cu surface after 24 h immersion in an anaerobic solution containing 0.1 M $\text{Cl}^- + 5 \times 10^{-5}$ M SH^- .

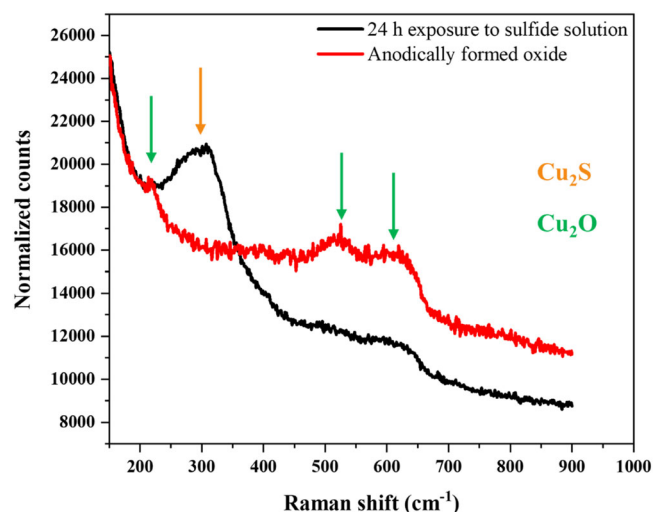


FIGURE 11 Raman spectra recorded on Cu samples preoxidized at -0.3 V/SCE in 0.1 M NaOH solution before and after 24 h immersion in a solution containing 0.1 M $\text{Cl}^- + 5 \times 10^{-5}$ M SH^- .

similar to those observed on Cu surfaces exposed to SH^- solution but not preoxidized.^[22,23] That Cu_2O was effectively converted to Cu_2S is confirmed by the Raman spectra in Figure 11. The preoxidized specimen not

exposed to an SH^- solution exhibited two broad peaks at 523 and 623 cm^{-1} and possibly also the minor peak at 220 cm^{-1} associated with Cu_2O .^[35,38] After 24 h of specimen exposure to SH^- solution, the spectrum is dominated by a broad peak at ~ 300 cm^{-1} , characteristic of Cu_2S .^[39,40] The shallow peaks attributable to Cu_2O may indicate residual traces of this phase.

3.5 | Conversion of $\text{Cu}_2\text{O}/\text{CuO}/\text{Cu}(\text{OH})_2$ to Cu_2S

The samples preoxidized in 0.1 M NaOH solution at -0.22 V/SCE were exposed to a 0.1 M $\text{Cl}^- + 5 \times 10^{-5}$ M SH^- solution for a series of exposure times. Figure 12a shows E_{corr} -time plots for samples exposed for 30 min and 24 h (only the first 300 min of exposure is shown here since there was no significant change over the subsequent exposure period), which exhibit a series of stages A–D. The initial E_{corr} in region A was 100 – 200 mV more positive than that registered when only a thin Cu_2O layer was present, Figure 8a. Before SH^- addition, consistent with the CSVs shown in Figure 5, a single peak attributable to the reduction of CuO and possibly Cu_2O was observed in the CSV. This high E_{corr} in region A

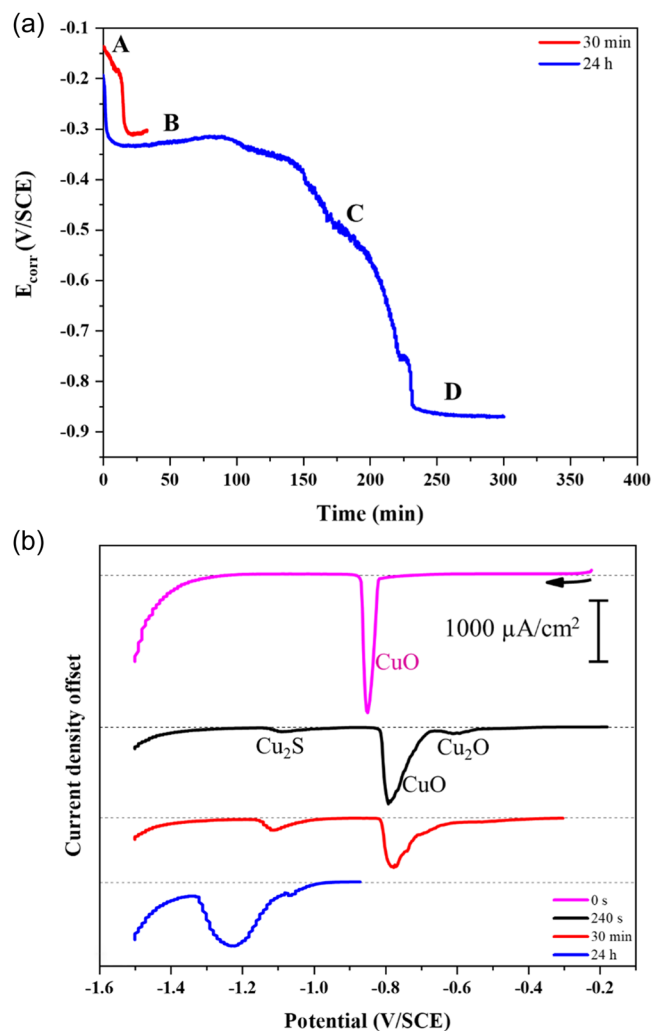


FIGURE 12 (a) E_{corr} recorded on Cu samples preoxidized at -0.22 V/SCE in 0.1 M NaOH solution after immersion in an anaerobic 0.1 M $\text{Cl}^- + 5 \times 10^{-5}$ M SH^- solution and (b) the respective CSVs performed at a scan rate of 1 mV/s after the surface was exposed to the sulfide for different time periods, as indicated.

suggests that the $\text{Cu}_2\text{O}/\text{CuO}$ film formed at -0.22 V/SCE was initially more protective and/or more oxidized than that formed at -0.3 V/SCE. Although the time required varied from ~ 2 to ~ 20 min, E_{corr} decreased to -0.35 V/SCE from -0.3 V/SCE, which was still ~ 100 mV more positive than observed after preoxidation at the lower potential.

A CSV recorded when E_{corr} had first decreased into region B (after 4 min of exposure) shows that the reduction of the $\text{Cu}_2\text{O}/\text{CuO}$ film occurred at a less negative potential, indicating a more reactive surface film. It is presently unclear what caused this shift in reduction potential, but it was likely due to an SH^- -induced change in the state of the surface film, indicated by the transition in E_{corr} from region A to region B, which rendered it more readily reducible. It is also noticeable that the reduction peak in Figure 12b is wider and less well defined. The observation of a small reduction peak at -1.05 V/SCE confirms that the formation of Cu_2S commenced in region B. At longer times in region B (after 30 min), the CSV shows that the $\text{Cu}_2\text{O}/\text{CuO}$ film became even easier to reduce, as the extent of Cu_2S formation increased, as indicated by the increase in the reduction peak current density at -1.12 V/SCE.

Once E_{corr} decreased into region D, a broad peak was observed in the CSV, confirming the presence of a significant amount of Cu_2S . This major broad reduction peak, preceded by a small shoulder, is characteristic of the reduction of a thin Cu_2S layer formed directly on the Cu surface, with a thicker layer of Cu_2S deposited on the outer oxide surface.^[22] In the present series of experiments, any change in behavior in region C was not captured. Previously, the stabilization of E_{corr} in this potential region was attributed to SH^- -induced porosity of the oxide film that enabled SH^- to penetrate the Cu surface and initiate galvanic corrosion via the coupling of reactions (3) and (4).^[27] This claim remains to be confirmed.

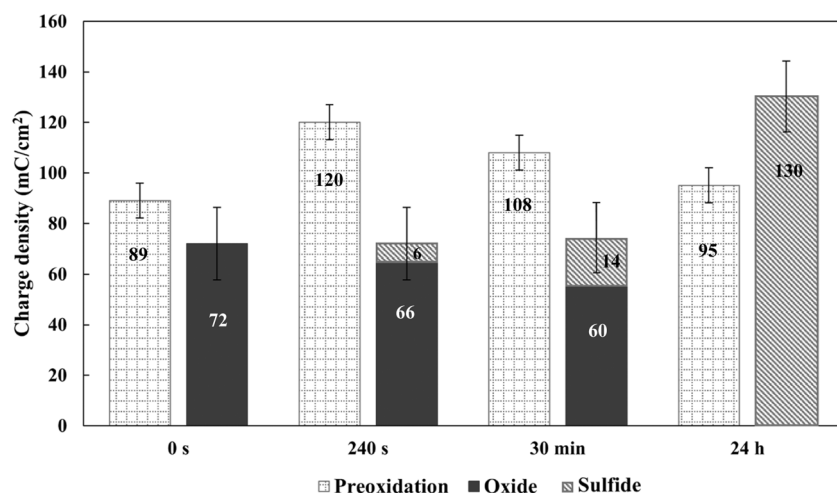


FIGURE 13 Anodic charge densities for samples preoxidized at -0.22 V/SCE in 0.1 M NaOH solution and the corresponding cathodic charges, with standard deviation, after immersion for different periods of time in a solution containing 0.1 M $\text{Cl}^- + 5 \times 10^{-5}$ M SH^- .

Figure 13 presents the anodic charges passed to create the oxide for each test run and the total amount of oxide and sulfide reduced during the CSV, expressed as charges obtained by the integration of the reduction peaks in the CSVs. The blank experiment was repeated under different conditions to determine the reason for the decrease in the cathodic charge compared with the corresponding anodic charge. Obtained results show that the 20% decrease in the total cathodic charge versus the anodic charge for the blank sample could be attributed to the presence of oxide/hydroxide species on the surface that could not be reduced in the CSV; the effect of rinsing with Type-I water was not noticeable here. Despite the differing amounts of anodic charge for sulfidized pregrown oxides at 240 s and 30 min, the same amount of cathodic charge (sum total of oxide and sulfide reduction) was measured from CSVs. It could be expected that preoxidation produced a reproducible base layer of Cu_2O and CuO , with most of the anodic charge beyond that level going to the growth of irreducible species on the surface, which likely includes poorly connected $\text{Cu}(\text{OH})_2$ species. The total amount of reducible Cu_2S after 24 h of immersion can be determined in the CSV, but whether or not there was any residual oxide on the surface cannot, since the poor electrical

connection between residual oxide/hydroxide and Cu substrate prevents it from being measured by CSV. Therefore, other complementary techniques are required to prove the presence of residual oxide on the surface. Over the first 30-min period, the sum total reduction charge for oxide and sulfide did not change significantly, suggesting that only oxide-to-sulfide conversion was occurring. However, over the much longer exposure period of 24 h, during which E_{corr} was in region D for the large majority of the exposure period, the charge for Cu_2S reduction was almost 1.5 times higher than that for creating the original oxide (considering 20% decrease in the cathodic charge for irreducible species), which is evidence that substantial oxidation of the Cu substrate, reaction (3), had occurred, in addition to oxide-to-sulfide conversion, reactions (3)–(5).

Figure 14 shows SEM micrographs of the surface and the cross section of a specimen exposed to a $0.1 \text{ M Cl}^- + 5 \times 10^{-5} \text{ M SH}^-$ solution for 45 min (region B in Figure 12a), and Figure 15 shows the corresponding EDX maps for Cu, O, and S. The crystalline nanowires formed during the preoxidation (and thought to be $\text{Cu}(\text{OH})_2$, Figure 6) appear to have remained mostly unconverted, as does the majority of the underlying $\text{Cu}_2\text{O}/\text{CuO}$ layer. The film thickness remained in the 100–300 nm range, as

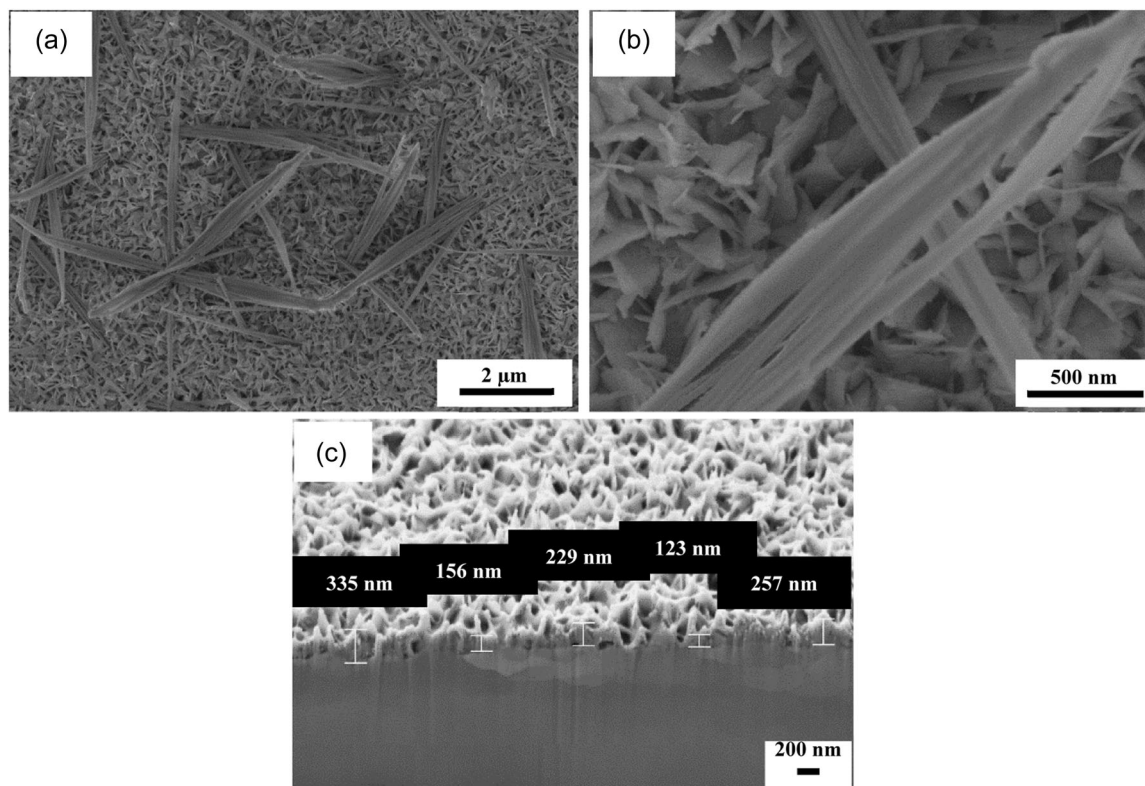


FIGURE 14 SEM micrographs (a, b) showing the surface morphology of an oxide film pregrown at -0.22 V/SCE in 0.1 M NaOH solution after 45 min exposure (stage B in E_{corr} plot vs. time, Figure 12a) to a solution containing $0.1 \text{ M Cl}^- + 5 \times 10^{-5} \text{ M SH}^-$; (c) an FIB-cut cross section of the film.

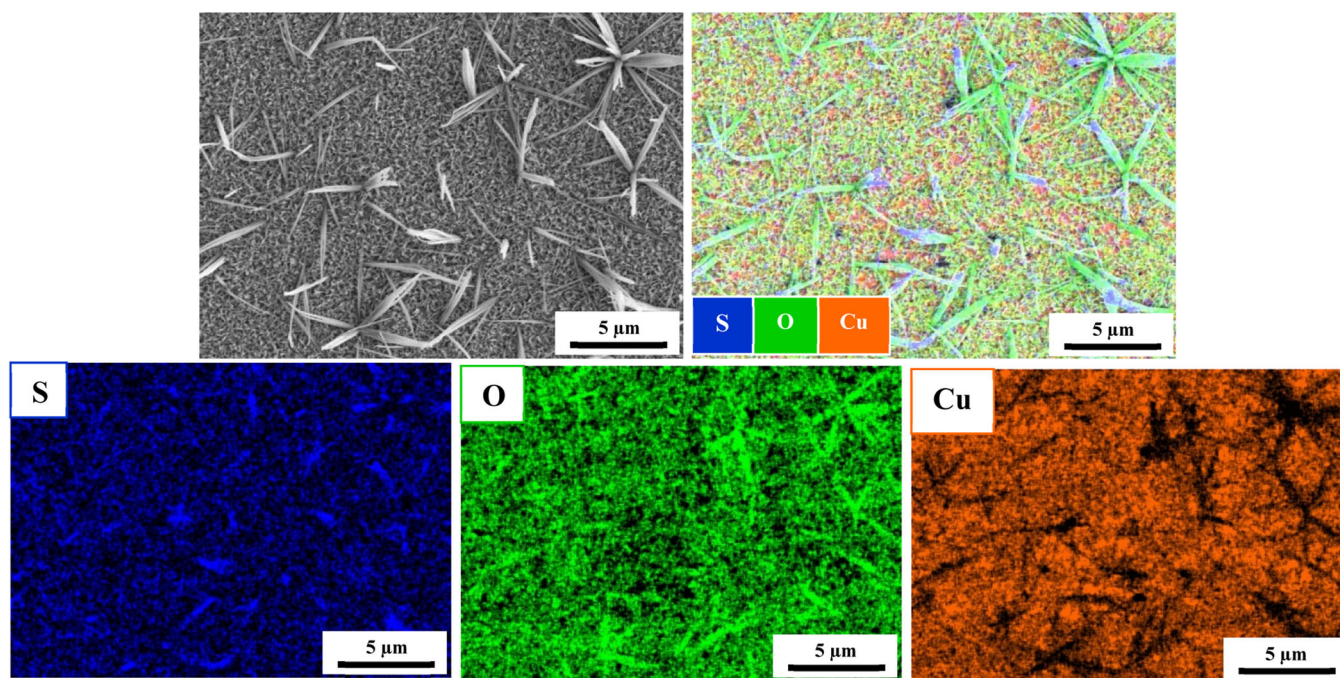


FIGURE 15 SEM micrograph and respective EDX maps of an oxide film pregrown at -0.22 V/SCE in 0.1 M NaOH solution after 45 min exposure (stage B in E_{corr} plot vs. time, Figure 12a) to a solution containing 0.1 M $\text{Cl}^- + 5 \times 10^{-5}$ M SH^- .

TABLE 2 Atomic percentage of different elements corresponding to Figure 15.

Element	Atomic (%)
Oxygen	47.1
Sulfur	0.8
Copper	52.1

observed for the preformed oxide film (Figure 6), confirming that no substantial additional Cu_2S formation had occurred. The EDX map for S, Figure 15, shows that the base layer of oxide experienced some apparently localized conversion to Cu_2S , consistent with the observation of only a small reduction peak at -1.0 V/SCE in the CSV after exposure in region B over such a period. It is also possible that the scattered locations exhibiting strong S EDX signals are associated with the locations of nanowires, which may indicate that their original growth during preoxidation occurred at more porous locations in the surface $\text{Cu}_2\text{O}/\text{CuO}$ layer. This would have allowed SH^- access to the Cu surface, leading to the direct formation of Cu_2S by reaction with Cu. That minimal conversion of oxide to sulfide occurred is confirmed by the elemental atomic percentages listed in Table 2, with approximately equal Cu and O percentages consistent with the dominant presence of CuO .

Figures 16 and 17 show a similar set of SEM images of the surface and cross section of a specimen exposed to

the SH^- solution for 24 h, that is, well into region D (as defined in Figure 12a). The surface and cross-sectional images show a widely dispersed deposit with an irregular morphology on top of a base layer which was thicker and more porous than that present on the preoxidized surface before exposure to the SH^- solution. The EDX maps suggest a significantly higher amount of S than observed after the short exposure, with the atomic percentages, Table 3, confirming this was the case. The high atomic percentage for Cu is consistent with the presence of Cu_2S , with the significant O percentage confirming that oxide-to-sulfide conversion was incomplete.

Inspection of the SEM images, Figures 16 and 17, shows that the majority of nanowire structures (thought to be $\text{Cu}(\text{OH})_2$) remained unconverted, although the presence of hexagonal crystals (indication of sulfide crystals by EDS analysis in Figure 17) at the tips of such structures suggest that conversion may have been underway at locations where the $[\text{SH}^-]$ was not depleted by reaction with the $\text{Cu}_2\text{O}/\text{CuO}$ sublayer and with the Cu substrate. Given that Cu_2S at these locations, like the irreducible oxide species, would have been in poor electrical contact with the Cu surface, it is likely they were not detected in CSV experiments. This would lead to an underestimation of the amount of Cu_2S present on the surface. Comparison of the Raman spectra recorded on a preoxidized specimen and on specimens exposed for either a short period (45 min; region B in Figure 12a) or a

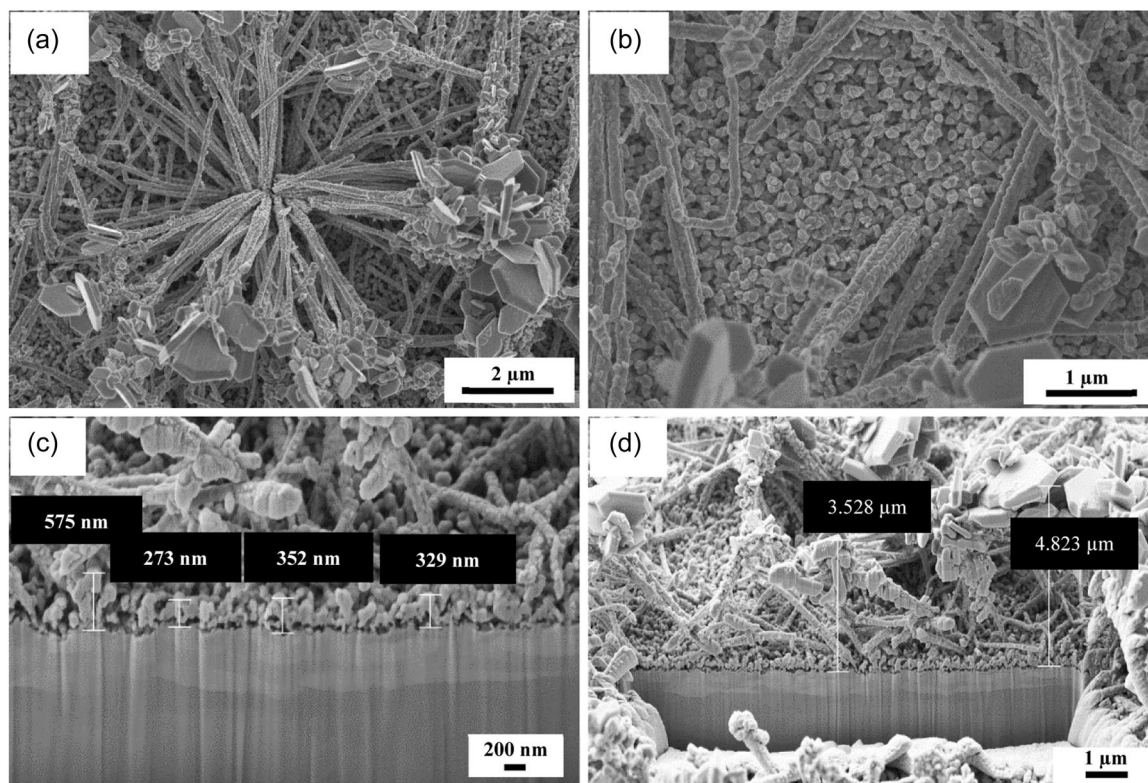


FIGURE 16 FE-SEM micrographs (a, b) showing the surface morphology of an oxide pregrown at -0.22 V/SCE in 0.1 M NaOH solution after 24 h exposure (stage D in E_{corr} plot vs. time, Figure 12a) to a solution containing 0.1 M $\text{Cl}^- + 5 \times 10^{-5}$ M SH^- and (c, d) an FIB-cut cross section of the film.

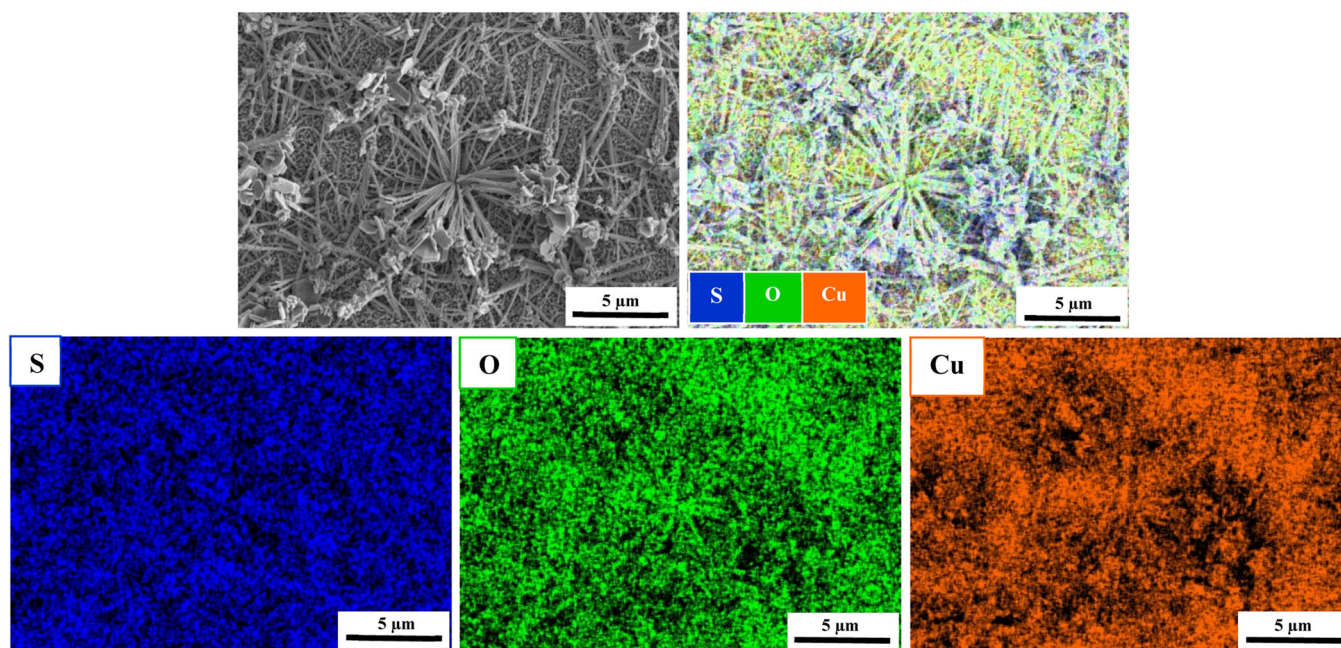


FIGURE 17 FE-SEM micrograph and respective EDX maps of an oxide pregrown at -0.22 V/SCE in 0.1 M NaOH solution after long-term exposure (stage D in E_{corr} plot vs. time, Figure 12a) to a solution containing 0.1 M $\text{Cl}^- + 5 \times 10^{-5}$ M SH^- .

TABLE 3 Atomic percentage of different elements corresponding to Figure 17.

Element	Atomic (%)
Oxygen	10.0
Sulfur	20.2
Copper	69.8

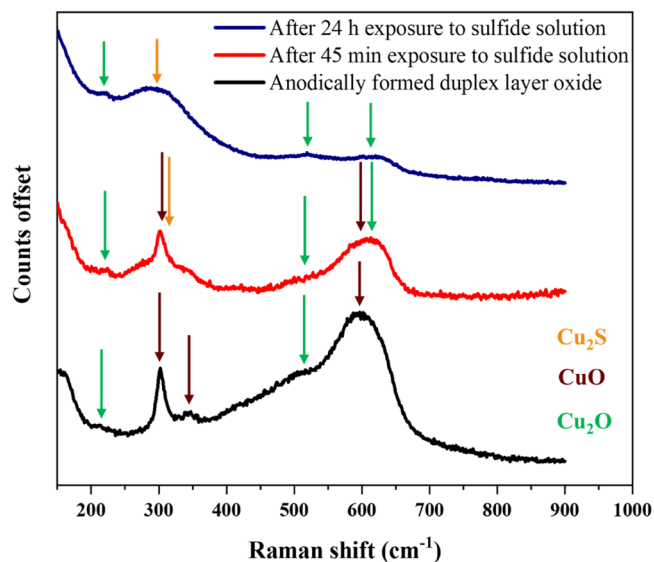


FIGURE 18 Raman spectra recorded on a Cu surface that was preoxidized at -0.22 V/SCE in 0.1 M NaOH solution before and after exposure to a solution containing 0.1 M $\text{Cl}^- + 5 \times 10^{-5}$ M SH^- for different periods.

long period (24 h; region D in Figure 12a), Figure 18, confirms that extensive conversion of the $\text{Cu}_2\text{O}/\text{CuO}$ surface layer occurred. Since Raman scattering is relatively insensitive to $\text{Cu}(\text{OH})_2$, its remaining presence in the nanowire structures could not be confirmed.

The data presented clearly demonstrate that when only a thin layer of Cu_2O was present on the Cu surface, its conversion to Cu_2S occurred rapidly, a process that could be attributed to the chemical conversion reaction (2), as previously claimed by Smith et al.^[27] However, when a mixed oxide/hydroxide ($\text{Cu}_2\text{O}/\text{CuO}/\text{Cu}(\text{OH})_2$) layer was present, complete conversion to Cu_2S was not achieved after 24 h of exposure to a solution containing 5×10^{-5} M SH^- . Initially, while the potential was in region A (Figure 12a) oxide-to-sulfide conversion, probably mostly Cu_2O to Cu_2S in the base layer, proceeded relatively easily. The penetration of SH^- to the Cu surface at a later stage could have initiated the galvanic coupling of CuO reduction (reactions (4) and (5) or reaction (6)) to Cu oxidation and Cu_2S formation (reactions (1)–(3)).

When the E_{corr} was in region B, where it stayed for an extended period, it is possible that a galvanic process,

required to convert Cu^{II} (in CuO) to Cu^{I} in Cu_2S , was accompanied by the chemical conversion of Cu_2O to Cu_2S (reaction (2)). Eventually, this combination of conversion processes led to the more extensive conversion of the $\text{Cu}_2\text{O}/\text{CuO}$ layer to Cu_2S and consequently the exposure of a larger surface area of the Cu substrate. This would have further accelerated the galvanic process, possibly accounting for the slight arrest in E_{corr} in region C (Figure 12a), and allowed the corrosion of the Cu substrate to Cu_2S via reaction (1). Whether or not the comproportionation reaction (6) was involved in the conversion of Cu^{II} to Cu^{I} remains unresolved.

Finally, the disperse outer layer of nanowires, which are assumed to be composed of $\text{Cu}(\text{OH})_2$, appears to have remained predominantly unconverted. This may reflect the possibility that this deposit was in poor electrical contact with the sublayers of $\text{Cu}_2\text{O}/\text{CuO}/\text{Cu}_2\text{S}$ and the Cu substrate, which would have inhibited the electron transfer process required to convert Cu^{II} to Cu^{I} . The accumulation of hexagonal crystals at the tips of the nanowires suggests that some conversion may have occurred. However, the formation of these crystals could be more plausibly attributed to the deposition of $\text{Cu}(\text{SH})_2^-$ and Cu_3S_3 species known to be released from a Cu surface corroding in an SH^- solution.^[41] Figure 19 shows an attempt to schematically illustrate the various stages of the overall conversion process.

4 | SUMMARY AND CONCLUSIONS

- Cu specimens were preoxidized electrochemically. The conversion of the oxide/hydroxide films to chalcocite (Cu_2S) in a chloride solution containing sulfide was monitored by measurement of E_{corr} and CSV.
- Thin Cu_2O films were rapidly converted to Cu_2S by a direct chemical reaction of the oxide in the presence of SH^- , indicating the importance of the structure and the thickness of Cu_2O in determining the efficiency of the conversion.
- The conversion of thicker duplex films composed of Cu_2O , CuO , and presumably $\text{Cu}(\text{OH})_2$ was considerably slower and remained incomplete over the longest exposure period of 24 h.
- The conversion of duplex films proceeded by a combination of chemical conversion (Cu_2O to Cu_2S) and a galvanic process involving oxide reduction (CuO to Cu^{I}) coupled to Cu oxidation (Cu to Cu_2S). The small amounts of $\text{Cu}(\text{OH})_2$ present did not appear to have been converted to Cu_2S during the longest exposure period (24 h).
- Since these conversion processes led to an increasing exposure of the underlying Cu substrate, the corrosion

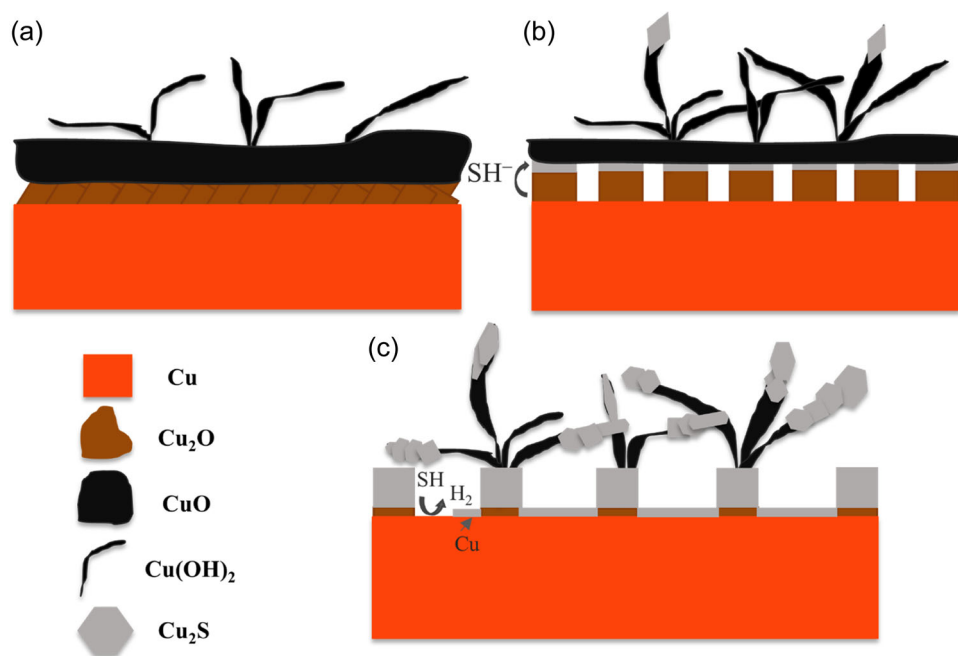


FIGURE 19 Schematic illustration of the stages of conversion of a $\text{Cu}_2\text{O}/\text{CuO}/\text{Cu}(\text{OH})_2$ film on a Cu surface to Cu_2S in a chloride solution containing $5 \times 10^{-5} \text{ M SH}^-$: (a) the $\text{Cu}_2\text{O}/\text{CuO}/\text{Cu}(\text{OH})_2$ layer before exposure to the SH^- solution; (b) the partially converted film after a short exposure period with E_{corr} in region B (Figure 12a); (c) the film after an extended period of exposure to the SH^- solution with E_{corr} in region D (Figure 12a).

process eventually became dominated by the direct oxidation of Cu to Cu_2S .

ACKNOWLEDGMENTS

This work was jointly funded by the Natural Sciences and Engineering Research Council of Canada, the Swedish Nuclear Fuel and Waste Management Company (SKB, Solna, Sweden), and the Nuclear Waste Management Organization (Toronto, Canada) through Alliance Grant ALLRP561193-20. The authors would like to thank Dr. Todd Simpson (Western Nanofabrication Facility) for his assistance with SEM/FIB and our colleague, Dr. Sina Matin, for his help with FE-SEM/EDX analyses (Surface Science of Western).

CONFLICT OF INTEREST STATEMENT

The authors declare no conflict of interest.

DATA AVAILABILITY STATEMENT

The data that support the findings of this study are available on request from the corresponding author. The data are not publicly available due to privacy or ethical restrictions.

ORCID

Elham Salehi Alaei  <http://orcid.org/0000-0003-3650-8765>

Jian Chen  <http://orcid.org/0000-0003-4021-7127>

Christina Lilja  <http://orcid.org/0000-0002-4338-5874>

REFERENCES

- [1] S. Sadekin, S. Zaman, M. Mahfuz, R. Sarkar, *Energy Procedia* **2019**, *160*, 513.
- [2] D. S. Hall, M. Behazin, W. J. Binns, P. G. Keech, *Prog. Mater. Sci.* **2021**, *118*, 100766.
- [3] F. Garisto, *Sixth Case Study: Features, Events and Processes*, Technical Report, NWMO-TR-2017-08, Nuclear Waste Management Organization, **2017**.
- [4] D. S. Hall, P. G. Keech, *Corros. Eng. Sci. Technol.* **2017**, *52*, 2.
- [5] T. Standish, J. Chen, R. Jacklin, P. Jakupi, S. Ramamurthy, D. Zagidulin, P. Keech, D. Shoesmith, *Electrochim. Acta* **2016**, *211*, 331.
- [6] L. Frizzell, Nuclear Waste Management Organization, *Implementing Adaptive Phased Management 2020 to 2024*, Technical Report, NWMO-2020-01, Nuclear Waste Management Organization, **2020**.
- [7] J. R. Scully, D. Féron, H. Hänninen, *Review of the NWMO Copper Corrosion Program*, Technical Report, NWMO-TR-2016-11, **2016**.
- [8] F. King, D. S. Hall, P. G. Keech, *Corros. Eng. Sci. Technol.* **2017**, *52*, 25.
- [9] P. Oy, *Safety Case for the Disposal of Spent Nuclear Fuel at Olkiluoto—Complementary Considerations 2012*, Technical Report, POSIVA 2012-11, **2012**.
- [10] F. King, C. Lilja, M. Vähänen, *J. Nucl. Mater.* **2013**, *438*, 228.
- [11] V. Ratia, L. Carpén, E. Isotahdon, C. Örnek, F. Zhang, J. Pan, *Corrosion of Copper in Sulphide Containing Environment: The Role and Properties of Sulphide Films—Annual Report 2019*, Technical Report, NKS-434, Nordic Nuclear Safety Research NKS, **2020**.
- [12] F. King, L. Ahonen, C. Taxen, U. Vourinen, L. Werme, *Copper Corrosion Under Expected Conditions in a Deep*

- Geologic Repository*, Technical Report, SKB-TR-01-23, Swedish Nuclear Fuel and Waste Management Co., **2001**.
- [13] R. Wu, R. Sandström, L. Z. Jin, *Mater. Sci. Eng. A* **2013**, 583, 151.
- [14] D. S. Hall, T. E. Standish, M. Behazin, P. G. Keech, *Corros. Eng. Sci. Technol.* **2018**, 53, 309.
- [15] F. King, M. Behazin, *Corros. Mater. Degrad.* **2021**, 2, 678.
- [16] J. Chen, Z. Qin, D. W. Shoesmith, *Corros. Eng. Sci. Technol.* **2011**, 46, 138.
- [17] F. King, *A Review of the Properties of Pyrite and the Implications for Corrosion of the Copper Canister*, Technical Report, TR-13-19, Svensk Kärnbränslehantering AB, **2013**.
- [18] L. Duro, V. Montoya, E. Colàs, D. García, *Groundwater Equilibration and Radionuclide Solubility Calculations*, Technical Report, NWMO TR-2010-02, Nuclear Waste Management Organization, **2010**.
- [19] Svensk Kärnbränslehantering AB, *Long-term Safety for the Final Repository for Spent Nuclear Fuel at Forsmark*, Technical Report, TR-11-01, Svensk Kärnbränslehantering AB, **2011**.
- [20] M. Guo, J. Chen, T. Martino, C. Lilja, J. A. Johansson, M. Behazin, W. J. Binns, P. G. Keech, J. J. Noël, D. W. Shoesmith, *Mater. Corros.* **2021**, 72, 300.
- [21] T. Martino, J. Smith, J. Chen, Z. Qin, J. J. Noël, D. W. Shoesmith, *J. Electrochem. Soc.* **2019**, 166, C9.
- [22] T. Martino, R. Partovi-Nia, J. Chen, Z. Qin, D. W. Shoesmith, *Electrochim. Acta* **2014**, 127, 439.
- [23] M. Guo, J. Chen, T. Martino, M. Biesinger, J. J. Noël, D. W. Shoesmith, *J. Electrochem. Soc.* **2019**, 166, C550.
- [24] J. Chen, Z. Qin, T. Martino, D. W. Shoesmith, *Corros. Eng. Sci. Technol.* **2017**, 52, 40.
- [25] P. T. Kristiansen, F. Massel, L. Werme, C. Lilja, L. C. Duda, *J. Electrochem. Soc.* **2015**, 162, C785.
- [26] F. King, M. Kolar, S. Stroes-Gascoyne, P. Maak, *MRS Online Proc. Libr.* **2003**, 807, 535.
- [27] J. M. Smith, J. C. Wren, M. Odziemkowski, D. W. Shoesmith, *J. Electrochem. Soc.* **2007**, 154, C431.
- [28] S. M. Abd El Haleem, E. E. Abd El Aal, *Corrosion* **2006**, 62, 121.
- [29] H. M. Hollmark, P. G. Keech, J. R. Vegelius, L. Werme, L. C. Duda, *Corros. Sci.* **2012**, 54, 85.
- [30] H. H. Strehblow, V. Maurice, P. Marcus, *Electrochim. Acta* **2001**, 46, 3755.
- [31] V. Maurice, P. Marcus, *Curr. Opin. Solid State Mater. Sci.* **2018**, 22, 156.
- [32] H. Chen, V. Maurice, L. H. Klein, L. Lapeire, K. Verbeken, H. Terryn, P. Marcus, *J. Solid State Electrochem.* **2015**, 19, 3501.
- [33] D. A. Palmer, *J. Solution Chem.* **2011**, 40, 1067.
- [34] M. Guo, J. Chen, C. Lilja, V. Dehnavi, M. Behazin, J. J. Noël, D. W. Shoesmith, *Electrochim. Acta* **2020**, 362, 137087.
- [35] G. Niaura, *Electrochim. Acta* **2000**, 45, 3507.
- [36] J. C. Hamilton, J. C. Farmer, R. J. Anderson, *J. Electrochem. Soc.* **1986**, 133, 739.
- [37] J. Chen, Z. Qin, D. W. Shoesmith, *Electrochim. Acta* **2011**, 56, 7854.
- [38] M. Liu, J. Li, *Materials* **2019**, 12, 2164.
- [39] A. Kudelski, *J. Raman Spectrosc.* **2003**, 34, 853.
- [40] J. R. Mycroft, G. M. Bancroft, N. S. McIntyre, J. W. Lorimer, I. R. Hill, *J. Electroanal. Chem. Interfacial Electrochem.* **1990**, 292, 139.
- [41] J. Chen, Z. Qin, T. Martino, D. W. Shoesmith, *Corros. Sci.* **2017**, 114, 72.

How to cite this article: E. Salehi Alaei, M. Guo, J. Chen, M. Behazin, E. Bergendal, C. Lilja, D. W. Shoesmith, J. J. Noël, *Mater. Corros.* **2023**, 74, 1690–1706. <https://doi.org/10.1002/maco.202313757>